Ann. Geophys. Discuss., https://doi.org/10.5194/angeo-2019-24
Manuscript under review for journal Ann. Geophys.
Discussion started: 27 February 2019

Spread F occurrence features at different longitudinal regions during low and moderate solar activity

Abimbola O Afolayan[1], Singh J Mandeep[1,2]*, Mardina Abdullah[1,2], Suhaila M Buhari[2,3], Tatsuhiro Yokoyama[4], Pornchai Supnithi[5]

[1] Center of Advanced Electronic and Communication Engineering, Universiti Kebangsaan Malaysia, 43600 Bangi, Selangor, Malaysia.

[2] Space Science Centre (ANGKASA), Institute of Climate Change, Universiti Kebangsaan Malaysia, 43600 Bangi, Selangor, Malaysia.

[3] Geomatic Innovation Research Group, Faculty of Science, Universiti Teknologi Malaysia, 81310 Johor Bahru, Johor, Malaysia.

[4] Research Institute for Sustainable Humanosphere, Kyoto University, Uji, Japan

[5] Faculty of Engineering King Mongkut's Institute of Technology Ladkrabang, Bangkok, Thailand

Correspondence to: Singh J. Mandeep (mandeep@ukm.edu.my)

Abstract

A comparative study of the equatorial spread F occurrence was conducted at different longitudes during 2009 or 2010 and 2011 or 2013 which represents the low (LSA) and moderate (MSA) solar activity periods respectively. The ionogram data were recorded at low latitude stations including Jicamarca (JIC; 75.76^{o}W, 8.17^{o}S), Peru; Fortaleza (FZA; 38.52^{o}W, 3.73^{o}S), Brazil; Ilorin (ILR; 7.55^{o}E, 9.93^{o}N), Nigeria; Chumphon (CPN; 88.46^{o}E, 11^{o}N), Thailand and Kwajalein (KWA; 167.73^{o}E, 8.72^{o}N), Marshal Island. The range type spread F (RSF) occurrence was manually recorded at an hour interval between 18:00 – 06:00 LT and a monthly average of the RSF occurrence was estimated for each of the seasons. The observed features of the RSF occurrence and its longitudinal distribution at different seasons include the difference in the onset time, duration and peak of occurrence. The significant observations include the asymmetric RSF occurrence distribution during the equinoctial season at most of the longitudes, while during the solstice seasons there are cases of discrepancy in the RSF occurrence with respect to the sunset terminator-magnetic field alignment. The inconsistent pattern of the RSF occurrence percentage and the post-sunset rise of the F layer in relation to the sunset time lag were analyzed. While the possible role of the seed perturbation

effect was discussed with respect to some of the peculiar features observed in the longitudinal/seasonal distribution of the spread F occurrence percentage.

Keywords: Equatorial Spread F; Vertical plasma drift; R-T instability; OLR.

1. Introduction

The equatorial spread F (ESF) is a nighttime phenomenon that describes the observed ionospheric F layer electron density irregularity within the equatorial or low latitude region and it is usually depicted as the widespread of the echo trace on the ionogram measurement (Booker and Wells, 1938; Bowman, 1990). This echo spread along the frequency band or height range is due to the scattered signal reflection from the multiple paths caused by the irregular ionospheric plasma density profile. The scale size of these plasma irregularities ranges between a few centimeters and hundreds of kilometer (Basu et al., 1978; De Paula et al., 2010). The ESF is usually initiated after the local sunset due to the rapid rise of the F layer and this generates a steep bottom-side plasma density gradient as a result of the abrupt reduction of the E region ionization level. The Raleigh-Taylor (R-T) instability excited in the bottom-side is considered as the mechanism responsible for the initiation and non-linear growth of the plasma depletion (Woodman and La Hoz, 1976). The pre-reversal enhancement (PRE) vertical drift velocity responsible for the uplift of the F layer in conjunction with the R-T instability mechanism is recognized as the basic drivers controlling the ESF morphology across different seasons and longitudes (Abdu, 2001; Dabas et al., 2003). The PRE rapidly elevates the ionosphere into a higher altitude region, where the collision frequency is lower and more conducive for further plasma depletion growth by the R-T instability mechanism.

The plasma irregularity occurrence around the equatorial/low latitude region causes distortion of the HF signal quality, thereby inducing a poor performance of the communication or navigation systems such as the Global Positioning System (GPS). Therefore, it is important to understand the role of the different precursory factors influencing the spread F morphology

Ann. Geophys. Discuss., https://doi.org/10.5194/angeo-2019-24
Manuscript under review for journal Ann. Geophys.
Discussion started: 27 February 2019

under varying ionospheric condition. This complex phenomenon has been explored widely by past studies and there are presently deliberate effort to improve the prediction accuracy of spread F occurrence distribution pattern across the different regions. The complex interaction between the E and F region dynamo system in the presence of conductivities and the magnetic field are responsible for the different electrodynamic phenomenon at the low latitude region. During the daytime, the F region divergent current causes an accumulation of the downward polarization electric field at the bottom-side of the region. On the other hand, the E region polarized electric field concurrently drives a closure current mapped along the magnetic field line into the F region that diminishes the F region vertical current (Abdu et al., 1981; Eccles et al., 2015; Heelis, 2004). The field line integrated Pedersen conductivity shorts out the F region dynamo electric field and significantly reduces the zonal plasma drift due to the high E region conductance during the daytime. However, the decay and the consequent reduction of the E region conductance during the nighttime causes a significant increase in the field-aligned Pedersen conductivity ratio. This generates a large vertical current by the F region dynamo and the resulting downward electric field drives the plasma in the direction of the neutral wind. Thus, the F layer dynamo electric field created by the divergence current dominates near the sunset period and this induces the eastward plasma motion in the F region at an $\boldsymbol{E} \times \boldsymbol{B}$ velocity. The PRE vertical plasma drift is associated with the enhanced eastward electric field caused by the significant decay of the E region conductivity. This combined with the rapid chemical recombination rate of the E layer around the sunset period results in the increased steepness of the bottom-side plasma density gradient and the initialization of the R-T instability.

The seasonal/longitudinal distribution of the ESF occurrence rate is dependent on the declination angle of the magnetic field. The longitudinal gradient of the field-aligned Pedersen conductivity becomes steepest when the sunset terminator is well aligned with the local magnetic flux tube, thereby resulting in a simultaneous relative sunset time at the magnetic conjugate E regions that are coupled to the F region (Abdu et al., 1992; Tsunoda et al., 2015). Hence, the eastward polarization electric field is maximum at such longitude and likewise the elevation of the F layer altitude near sunset. The base of the F region gets lifted to greater heights making it conducive for the plasma instability growth. Therefore, the longitudinal variation in the seasonal distribution of the ESF occurrence rate is associated with the variation of the solar terminator-magnetic field alignment (STBA) and their distinct local sunset time equatorial electric field system. Due to the near-zero sunset time lag between the conjugate E regions during the equinox period, there is usually a good alignment. On the other hand, the solstice months have been shown in several studies (Hoang et al., 2010; Su et al., 2008) to have good (bad) alignments during June solstice (December solstice) at longitudes of positive (negative) magnetic declination. The seasonal/longitudinal distribution of the equatorial plasma irregularity has been extensively reported to be strongly correlated with the seasonal variation of the STBA (Abdu et al., 1981; Li et al., 2008; Su et al., 2008). However, a recent study described the significant ESF occurrence during the solstice seasons at the West African and Central Pacific region to be inconsistent with the defined theory of the declination angle influence on the spread F longitudinal distribution (Tsunoda et al., 2015). Likewise, Huang, (2017) reported an anti-correlation between the vertical plasma drift and the small amplitude irregularity during the moderate solar activity period. These discrepancies are considered noteworthy for an improved understanding of the features of global plasma irregularity distribution as influenced by different background atmospheric conditions.

The main focus of this study is to examine the salient features of the spread F local time distribution patterns during the different seasons of the low and moderate solar activity at the different longitude sectors. Furthermore, the possible competing role of the vertical plasma drift, virtual height and the seed perturbation in the observed spread F distribution for the considered longitude sectors will be discussed.

Ann. Geophys. Discuss., https://doi.org/10.5194/angeo-2019-24
Manuscript under review for journal Ann. Geophys.
Discussion started: 27 February 2019

2. Data and methods

The ESF events were recorded at the equatorial stations situated at different longitudes (Jicamarca (JIC) station, Peru; Fortaleza (FZA) station, Brazil; Ilorin (ILR) station, Nigeria; Chumphon (CPN) station, Thailand and Kwajalein (KWJ) station, Marshal Island), as shown in Table 1. The table lists the geographic coordinates and the sunset time at each of the stations selected for the study of the spread F irregularity distribution. These are stations within the Southeast Asia low-latitude ionospheric network (SEALION) and Global Ionospheric Radio Observatory (GIRO) network as indicated in Figure 1. The observation data were taken using the digital ionosonde (DP-S 4 digisonde) and analogue type FMCW (frequency modulated continuous wave) (Maruyama et al., 2008; Reinisch and I. A. Galkin, 2011). Since the ESF events are very rare during the daytime, our investigation is limited to the time interval between 18:00 – 06:00 LT. Though the ionograms were recorded at different intervals at each of the stations, we analyzed the ionogram at 15 min interval during the nighttime hours, except that of the Fortaleza station which was set at 10 min interval. Each ionogram is examined for the presence of range spread F (RSF) or strong range spread F (SSF) according to the defined interval. Subsequently, the hourly variation of the RSF occurrence percentage was then estimated using the relation:

$$hourly\ occurrence\ \% = \frac{number\ of\ ionograms\ with\ ESF\ in\ the\ hour}{total\ number\ of\ ionograms\ in\ an\ hour\ over\ the\ month} \times 100 \qquad (1)$$

Only the quiet days ($k_p \leq \Sigma 24$) were considered for each month representing the different seasons during the low (F107A < 100 sfu) and moderate (F107A < 150 sfu) solar activity period (Wang et al., 2017). The seasonal variation of the ESF events across the different longitudes was analyzed according to the available data at each station. Thus, the data taken from April, June, September and December months of 2010 (2013) represents the March equinox, June solstice, September equinox and December solstice of LSA (MSA) respectively.

Ann. Geophys. Discuss., https://doi.org/10.5194/angeo-2019-24
Manuscript under review for journal Ann. Geophys.
Discussion started: 27 February 2019

Table 1: Description of the stations' geographic location and their local sunset time range.

Station	Longitude (degree)	Latitude (degree)	Dip Latitude	Declination angle	Sunset time (LT)
Jicamarca	-75.76	-8.17	3.75	-3.24	18:45 – 19:15
Fortaleza	-38.52	-3.73	-6.89	-20.11	18:30 – 18:45
Ilorin	4.5	8.53	-4.27	-1.69	18:00 – 19:00
Chumphon	99.37	11	3.76	-1.46	19:30 – 20:15
Kwajalein	167.73	8.72	3.62	7.62	19:30 – 20:15

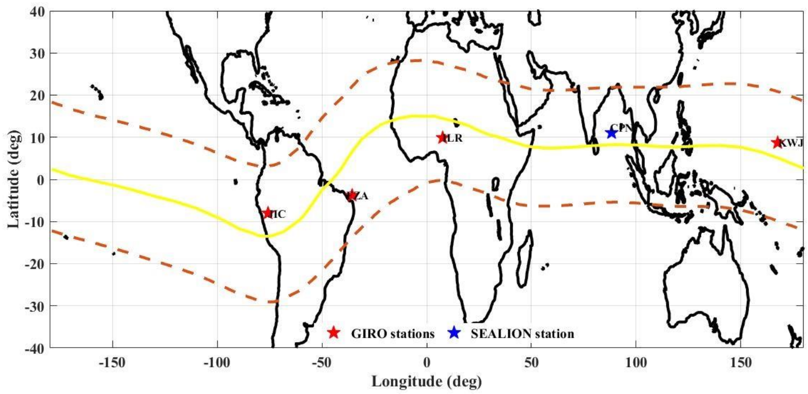

Figure 1: The geomagnetic location of the ionosonde stations and their corresponding observatory network shown by the red (GIRO) or blue (SEALION) marker.

The recorded ionogram echo spread signatures are usually divided into frequency spread F (FSF), mixed spread F (MSF), range spread F (RSF) and strong range spread F (SSF) (Shi et al., 2011). However, this study considers only the RSF and SSF type during the manual observation of the plasma irregularities across these longitudes. The RSF signature represents the instance of the echo spreading mainly along the height axis as shown in Figure 2, while the SSF is described as a type of RSF with the F layer trace echo significantly extending beyond the local foF2. Hereafter, we will refer to both types of spread F as RSF, while the March, June, September and December seasons regarded as M-equinox, J-solstice, S-equinox and D-solstice respectively.

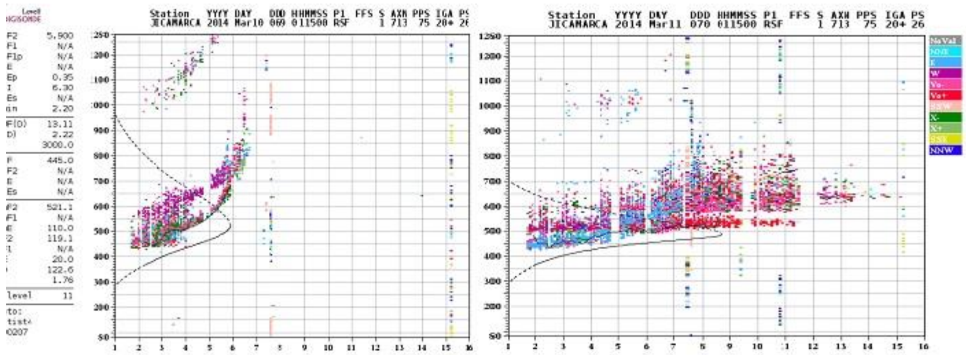

Figure 2: Sample of the RSF (left) and SSF (right) recorded using the DPS-4 digisonde at the Jicamarca station.

The monthly average of the scaled virtual height was taken as a representation of the seasonal variation of the near sunset vertical plasma drift recorded at each of the ionosonde stations. The seasonal variation of the virtual height taken during the low solar activity (LSA) and moderate solar activity (MSA) period was then analyzed in correspondence to the RSF occurrence distribution. Based on data availability across the considered stations as shown in Figure 3, the data taken during the year of 2009 or 2010 represents the LSA period while the year of 2011 or 2013 is taken for the MSA period. Since the solar flux unit is similar, we consider it acceptable to make a comparison between the RSF occurrence pattern during the mentioned years for the LSA and MSA period.

Figure 3: The ionogram data availability at the Jicamarca, Fortaleza, Ilorin, Chumphon and Kwajalein stations during the (a) LSA and (b) MSA period.

3. Results

Figures 4 and 5 present the nighttime hourly variation of the monthly mean of the RSF occurrence percentage across the different longitudes during the LSA period and the MSA period based on the available data at the different stations. The seasonal variation of the RSF occurrence pattern across the different longitude regions was represented as a histogram of the spread F occurrence rate during the LSA and MSA period. Generally, the average duration of the post-sunset plasma irregularity in Figure 4 varies across the longitude, while the start time of the spread F varies mostly between 18:00 and 20:00 LT during the equinox and D-solstice months. The observed variation in the start time of the RSF occurrence corresponds with the varying sunset time across the different longitudes as shown in Table 1. The monthly average of the RSF occurrence percentage is higher at all the considered longitudes during the equinox months than the solstice months of the LSA year. The percentage of RSF occurrence and duration is highest at the ILR station for all the seasons, while the average lowest occurrence percentage was recorded at the CPN station. Li et al., (2011) showed that most post-midnight plasma irregularity occurrence in the African region were initiated during the post-sunset period. It is also important to highlight the significantly high probability of RSF occurrence at the ILR and KWJ stations during the J-solstice month of the LSA year. Unlike the other longitude regions where the RSF occurrence is below 10% during this period. Furthermore, the plasma irregularity onset time during the M-equinox and J-solstice at the KWJ station was delayed by ~2hrs after the local sunset time.

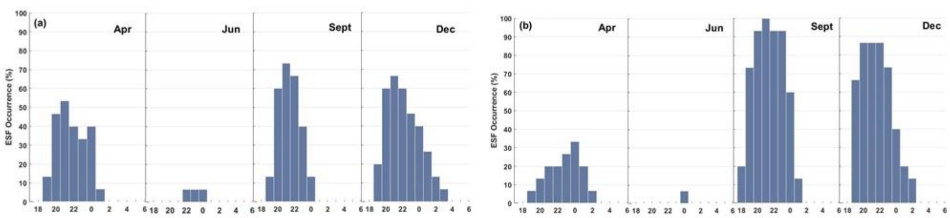

Ann. Geophys. Discuss., https://doi.org/10.5194/angeo-2019-24
Manuscript under review for journal Ann. Geophys.
Discussion started: 27 February 2019

Annales Geophysicae Discussions
Open Access

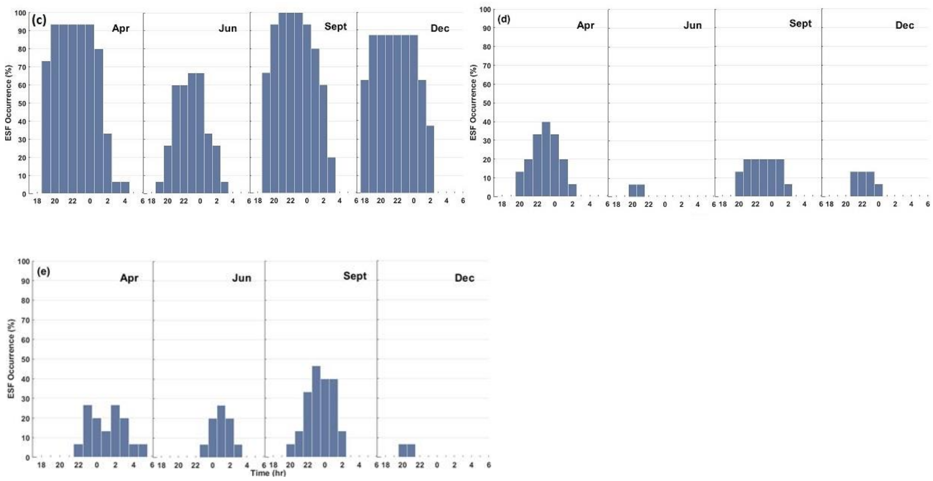

Figure 4: Occurrence rate of RSF during LSA period at the (a) Jicamarca (b) Fortaleza (c) Ilorin (d) Chumphon and (e) Kwajalein stations.

Figure 5, shows that there was more than 50% increase in the RSF occurrence percentage during the M-equinox months of the MSA period across all the stations except at the ILR station, where ~100 % was already recorded during the LSA. The spread F equinox asymmetry was very visible in all the regions except at the FZA station. The RSF occurrence percentage hourly peak was approximately the same at both equinox seasons at the FZA station. Unlike the equinox asymmetry pattern observed during the LSA period, the M-equinox has a significantly higher RSF occurrence percentage at the CPN, JIC and KWJ stations. Figures 4 and 5, show the similarity between the observed RSF occurrence percentage during the solstice months of both solar epochs. The RSF occurrence percentage during the J-solstice of the MSA period was lesser than or ~10% at all the stations except at the KWJ station. Likewise, there was ~30% increase in the recorded RSF occurrence percentage at the KWJ station during J-solstice and the irregularity onset time was also much earlier (immediately after the local sunset) than the LSA onset time. The pre-midnight RSF occurrence percentage peak recorded ~15% increase at the FZA and CPN stations during the D-solstice, while there was no occurrence of RSF at the KWJ station. The largest STBA is observed at the negative declination

Ann. Geophys. Discuss., https://doi.org/10.5194/angeo-2019-24
Manuscript under review for journal Ann. Geophys.
Discussion started: 27 February 2019

Annales Geophysicae Discussions

angle region during the D-solstice, correspondingly the highest RSF occurrence percentage peak was recorded at the FZA station for both the LSA (~85%) and MSA (~100%) period.

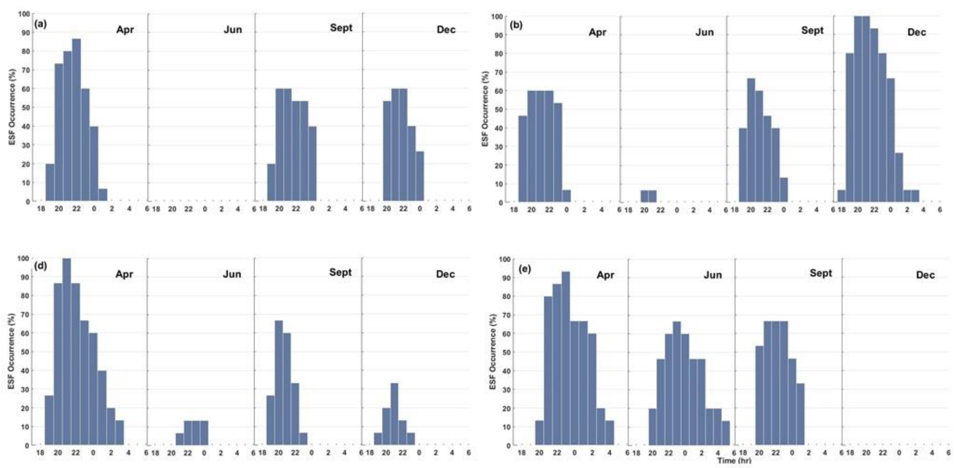

Figure 5: Occurrence rate of RSF during the MSA period at the (a) Jicamarca (b) Fortaleza (d) Chumphon and (e) Kwajalein stations.

Figure 6(a-d) shows a comparison of the ESF occurrence percentages during the MSA and LSA at each of the four stations with sufficient data. There was a significant difference between the spread F occurrence percentage during the LSA and MSA period across all seasons at most of the stations except at the JIC and FZA stations. The ESF occurrence percentage at both stations were inversely related to the solar flux index during S-equinox and approximately the same during the D-solstice of both solar epochs. The observed pattern in the occurrence rate at the Brazilian longitude might be attributed to the fact that the average ESF occurrence percentage in this region is typically high (Su et al., 2007). Furthermore, the S-equinox and D-solstice seasons offer the most favourable conditions for the generation of ESF at this longitude region. Hence, the ESF occurrence percentage as observed in Figure 6(b) is independent of the solar activity index during the S-equinox and D-solstice period. The non-occurrence of RSF at the JIC station presents a similar pattern as the earlier recorded decrease in the plasma irregularity occurrence percentage with respect to an increasing solar flux index in this

Ann. Geophys. Discuss., https://doi.org/10.5194/angeo-2019-24
Manuscript under review for journal Ann. Geophys.
Discussion started: 27 February 2019

longitude region (Li et al., 2011). Such anti-solar activity alignment of the RSF occurrence during the solstice seasons have been discussed by Su et al., (2007) and attributed to the neutral wind effect. Their result was corroborated by the diverging neutral meridional wind observed during the J-solstice in this longitude and the expected influence of the increased meridional wind during the MSA. The peak ESF occurrence percentage at most of the longitudes during the LSA is usually around the midnight period while in the case of the MSA, the peak is closer to the local sunset time. However, thorough consideration of the observed ESF occurrence features during LSA as shown in Figures 6(a-b) indicated that the near sunset peak and the rapid increase of the occurrence percentage were more consistent with the seasons having a significant PSSR rather than the solar flux index. The typical plasma irregularities formed around the sunset period are dominated by the PRE dynamics, while some other mechanisms may play a substantial role in the post-midnight ESF events.

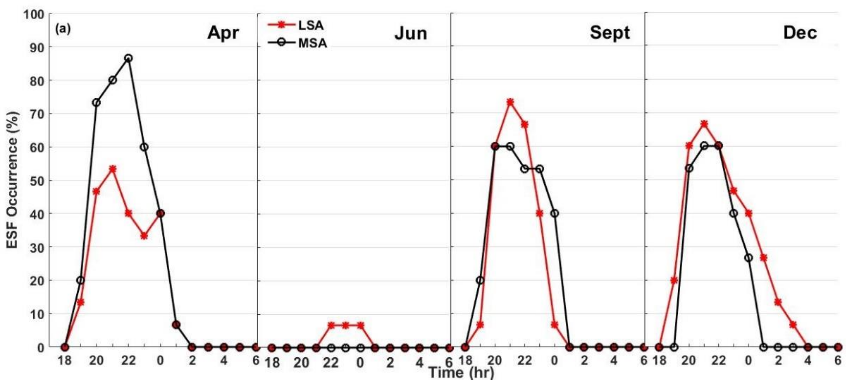

Ann. Geophys. Discuss., https://doi.org/10.5194/angeo-2019-24
Manuscript under review for journal Ann. Geophys.
Discussion started: 27 February 2019

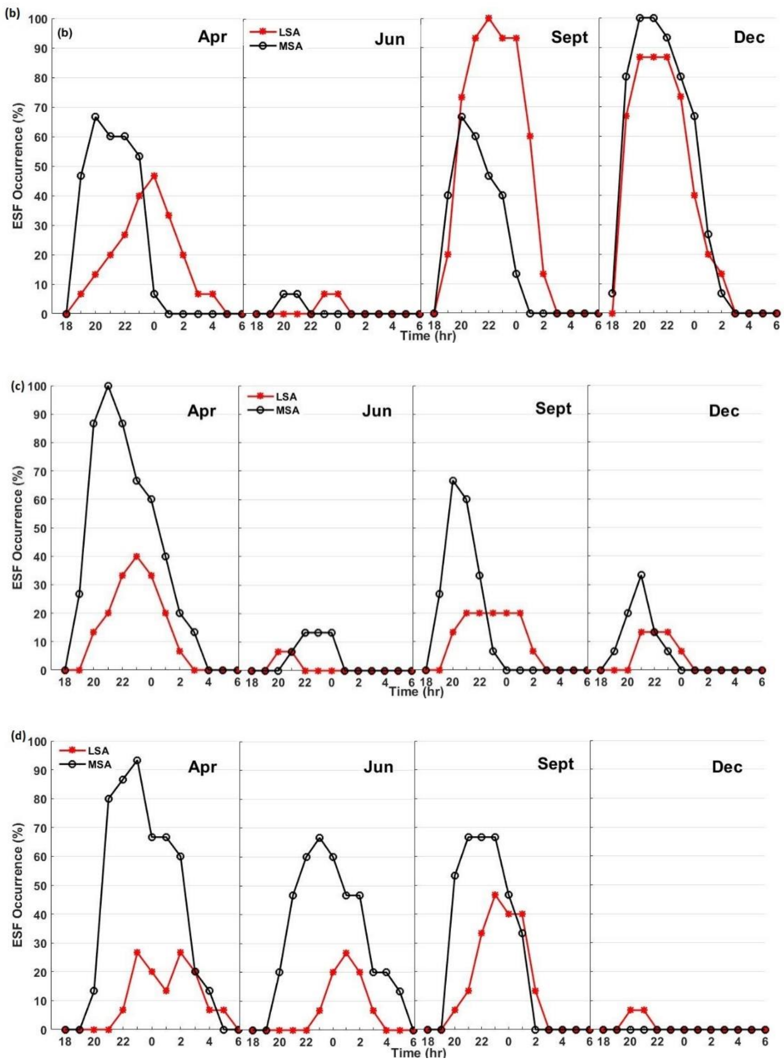

Figure 6: The percentage of ESF occurrence during the LSA and MSA period for (a) JIC (b) FZA (c) CPN and (d) KWJ stations.

Figures 7(a) & (b). show the local time variation of the monthly mean virtual height ($h'F$) during the LSA and MSA period across the five longitude regions considered in this study. Likewise, the corresponding annual variation of the sunset time lag was also presented in Figure 7(c). This represents the difference between the local sunset times at the foot-points of the conjugate E region that connects with the F layer base. The longitudinal variation pattern

Ann. Geophys. Discuss., https://doi.org/10.5194/angeo-2019-24
Manuscript under review for journal Ann. Geophys.
Discussion started: 27 February 2019

Annales Geophysicae Discussions

of the PSSR is consistent with the earlier numerical simulation by Vichare and Richmond, (2005), which observed that the longitudinal PRE variation have its peak between 290^o E and 30^o E longitude region. The observed post-sunset rise of the $h'F$ (representing the evening pre-reversal enhancement (PRE) of the vertical plasma drift) is generally higher during the equinoctial and D-solstice months of MSA than the corresponding seasons of the LSA period. In the case of J-solstice months, the near sunset enhancement of the vertical plasma drift was almost absent during both LSA and MSA period. Though based on our comparison with the annual sunset time lag variation for each of the regions as shown in Figure 7(c) , the PRE magnitude was expected to be larger at the KWJ station than the other regions. However, the magnetic field strength in the Asian (CPN) and Central Pacific (KWJ) region is quite large (Su et al., 2009; Vichare and Richmond, 2005) and this was responsible for the weak PRE mostly observed in this regions during both MSA and LSA period. Such zonal variation of the different factors including the zonal wind, eastward electric field and magnetic field strength contributes to the resultant zonal variation of the vertical plasma drift amplitude across the longitude sectors. Our comparison of the sunset time lag with the corresponding PSSR of the *h'F* also highlights an inconsistent pattern in the form of solstice asymmetry at the low declination angle regions. Similar asymmetry is also prominent during the equinoctial seasons of the MSA at all the regions except the KWJ station where we earlier recognized the inverse effect of the strong magnetic field intensity on the post-sunset PRE vertical drift. The equatorial electrojet (EEJ) was identified as a likely controlling factor in the seasonal variation of the PSSR, while the monthly modulation in the F region eastward neutral wind velocity was found insufficient to describe the observation (Tsunoda et al., 2015). The EEJ effect is as a result of the strong dependence of the PSSR on the longitudinal gradient of the Pedersen conductivity. Hence, a seasonal modulation of the EEJ strength by tidal winds from the lower atmosphere will contribute to the PRE. Similarly, Su et al., (2009) highlighted the influence of the prolonged eastward EEJ on the zonal drift reversal during J-solstice. Which is expected to be accompanied by a weak vertical plasma drift in the F region.

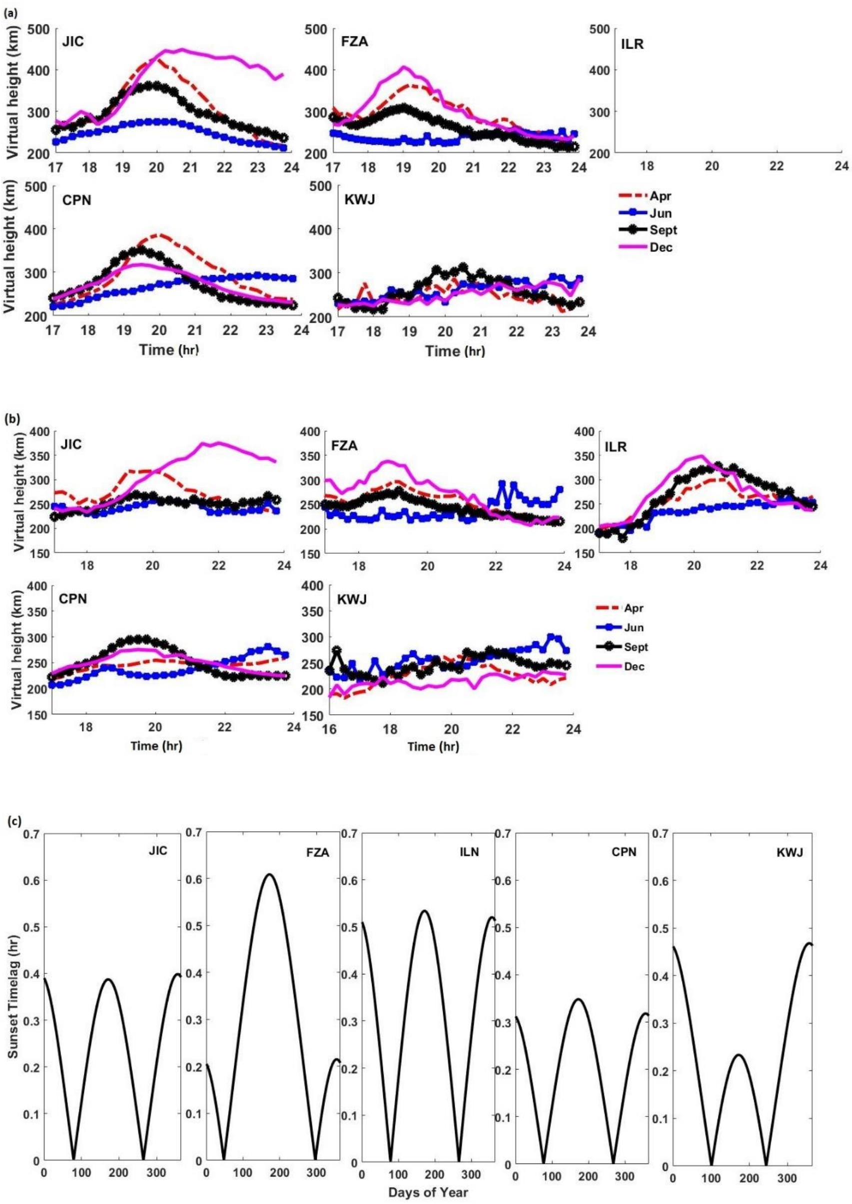

Figure 7: Monthly average of the virtual height during (a) LSA, (b) MSA and (c) The estimated sunset time lag between the geomagnetic conjugate points for each of the longitude sectors.

Ann. Geophys. Discuss., https://doi.org/10.5194/angeo-2019-24
Manuscript under review for journal Ann. Geophys.
Discussion started: 27 February 2019

4. Discussion

A comparison between our observation and the earlier investigations (Klinngam et al., 2015; Pezzopane et al., 2013; Pietrella et al., 2017; Su et al., 2007; Tsunoda et al., 2015) on the spread F occurrence pattern across these longitudes shows a strong similarity during the different seasons of the MSA and LSA period. These previous studies have deployed different measurement techniques to establish a strong linear relationship between the eastward electric field enhancement near the sunset and the seasonal/longitudinal distribution of the spread F occurrence across the solar epoch (Fejer et al., 1999; Huang, 2018; Stolle et al., 2008; Whalen, 2002). The R-T instability mechanism is considered responsible for the plasma irregularity initiation and the observed seasonal variation pattern. This is controlled by the flux tube integrated conductivities of the E and F regions ($\Sigma_F^P \; and \; \Sigma_E^P$) and other parameters as shown below (Ossakow, 1981; Sultan, 1996);

$$\gamma = {\Sigma_F^P}/{\Sigma_F^P + \Sigma_E^P} \times \left({g}/{V_{in}} + U_n^p + V_Z \right) \times {1}/{L} - \beta \quad (2)$$

Where V_Z is the vertical plasma drift component of the $E \times B/B^2$ and U_n^p is the vertical component of the neutral wind perpendicular to the magnetic field. While β is the recombination rate. g is the acceleration due to gravity and V_{in} is the collision frequency.

The PRE of the zonal electric field around the local sunset is responsible for the uplift of the F layer into the altitudinal region suitable for the rapid plasma irregularity growth by the R-T instability mechanism. Thus, PRE was described as a dominant factor influencing the difference in the observed features such as the onset time, occurrence rate or latitudinal extension of the plasma irregularity across the various season or longitude. An example of such control is the observed delay (2 hours lag) in the RSF occurrence onset time during the LSA compared to the observed characteristics during the MSA period at the KWJ station shown in Figure 4. This is attributed to the delay in the zonal drift reversal time and the weaker zonal neutral wind magnitude during the LSA (Su et al., 2009). As a result of the reduction in the zonal wind and conductivity gradient, which is expected to cause a difference between the near sunset vertical drift pattern of the two solar epochs. Su et al., (2009) presented their analysis on the zonal drift reversal effect on the post-sunset dynamics at the F region base using the simulation result obtained during the J-solstice season. Thus, further investigation might be required to confirm whether same factors were responsible for the significant difference between the onset time observed during the M-equinox seasons of both solar epochs at the KWJ station as shown in Figure 4(e). On the other hand, the high RSF occurrence percentage at some of the regions during the LSA with a corresponding weak post-sunset PRE indicates a significant contribution by other factors. Though Smith et al., (2016) have attributed such significant RSF occurrence percentage during the LSA to the effect of the requisite PRE threshold for the plasma irregularity initiation being directly dependent on the solar flux index. It was explained that a much lesser PRE peak is required for the uplift of the F region base into a region with reduced ion-neutral collision frequency due to the contracted ionosphere during the LSA period. However, as the density scale length (L) is inversely related to the instability growth rate, we presume that the reduced L during LSA is conducive for a faster linear instability growth in response to a strong seeding effect (Huang and Kelley, 1996).

The equinox and solstice asymmetry observed in the ESF occurrence percentage at all the longitude regions during both solar epochs appears to be controlled by different mechanisms entirely. In the case of the equinox asymmetry, the occurrence percentage is higher during the S-equinox at the JIC, FZA and KWJ stations during the LSA period. While the M-equinox is higher at the CPN station and the ILR station shows approximately the same occurrence percentage during both equinoctial seasons. The equinox asymmetry is most visible at the Brazilian and Peruvian longitude during the LSA. Most of the regions as shown in Figure 7a, typically present a deviation between the RSF occurrence percentage asymmetry and the approximately equal *h'F* peak at both equinoxes during the LSA. In contrast, the equinoctial asymmetry of the RSF occurrence during the MSA as shown in Figure 7(b). conforms with the corresponding larger *h'F* peak during the M-equinox season at these stations. Manju and Madhav Haridas, (2015) related the observation of equinox asymmetry in threshold height ($h'F_c$) and ESF occurrence percentage to the equinox asymmetry in the O/N_2 ratio. This asymmetry was shown to have a strong solar flux dependence. They associated that with a significant difference between the expansion of the thermosphere at both equinoxes as the solar flux increases, which expectedly reflects on the defined $h'F_c$. The relationship between the thermospheric neutral compositions and the post-sunset dynamics of the F region have been shown by the earlier studies (Batista et al., 1986; Qian et al., 2009). The neutral density in the upper thermosphere is known to change with a variation in the O/N_2 ratio, and the post-sunset vertical drift was established to have a directly proportional relationship with the neutral density. Thus, the higher O/N_2 ratio during the M-equinox as reported by Manju and Madhav Haridas, (2015) is expected to correspond to a higher vertical drift peak during this period. Figure 7(b). presents a similar pattern in the estimated PSSR during the equinoctial months. The observed difference in the *h'F* peak is more significant during the MSA, while during the LSA period, the observed PRE peak was approximately equal for both equinoxes across the different regions. This shows a comparably similar pattern with the observed equinoctial asymmetry in the occurrence percentage and duration of RSF for all the regions except in the Brazilian region (represented in Figures 4 and 5). From Figure 4, the Brazilian region recorded a large difference between the occurrence rate of RSF during the equinox seasons of the LSA period and the higher percentage was during the S-equinox season. On the other hand, the RSF occurrence percentage peak was approximately the same for both equinox seasons during the MSA period. Furthermore, an anti-solar activity dependence of the RSF occurrence percentage was also observed at the JIC and FZA stations during the S-equinox as shown in Figures 6(a-

Ann. Geophys. Discuss., https://doi.org/10.5194/angeo-2019-24
Manuscript under review for journal Ann. Geophys.
Discussion started: 27 February 2019

Annales Geophysicae Discussions

b). Similar anti-solar activity pattern was observed at this longitude region by Su et al., (2007) but less prominent than our result due to the difference in the altitude of data observation. We assume that this resulted from a combined effect of the large RSF occurrence percentage in this longitude regions during the LSA and the increased bottom-side density scale length (Lee, 2010) as compared to the insignificant difference in the PRE during both epoch. The inconsistency in the equinoctial asymmetry pattern at different solar flux index was also observed in the Atlantic region during the study of the global equatorial plasma bubble occurrence (Gentile et al., 2006).

During the solstice seasons, the observed asymmetry in the PRE of the F layer and the RSF occurrence percentage at the low declination angle longitudes are inconsistent with the corresponding sunset time lag. Unlike the FZA and KWJ stations where the asymmetry between the solstices could be explained by the difference in the sunset time lag, these three longitudes have approximately the same sunset time lag at both solstices. Hence, we discuss the probable role of GW in the recorded ESF occurrence percentage, especially during the LSA. The seeding effect is considered an important parameter in the analysis of the plasma irregularity generation during days characterized by a weak ambient ionospheric condition as observed across most regions. A direct link was established between the GW from the intertropical convergence zone (ITCZ) and the frequency of ESF activity using the outgoing longwave radiation (OLR) data (Ogawa et al., 2006; Tsunoda, 2010c). The seeding of the ionospheric density perturbation is expected to occur when the ITCZ is located near the dip equator (Tsunoda, 2010a). Which raised a discussion about the GW phase front and magnetic field line alignment (GWBA) hypothesis. This combined with the STBA theory was considered important to form a complete description of the seasonal morphology of ESF occurrence across different longitude (Tsunoda, 2010a). The geographic map of the OLR measurement provides the longitudinal distribution of the deep convective activity (Gu and Zhang, 2002; Waliser and

Ann. Geophys. Discuss., https://doi.org/10.5194/angeo-2019-24
Manuscript under review for journal Ann. Geophys.
Discussion started: 27 February 2019

Gautier, 1993). The seasonal variation of the GW occurrence across the different regions will then be analyzed using the interpolated OLR data that are available from the National Oceanic and Atmospheric Administration NOAA website (http://www.esrl.noaa.gov/psd/data/gridded/data.interp_OLR.html). Which will be compared with the observed seasonal variation of the ESF occurrence percentage across these regions.

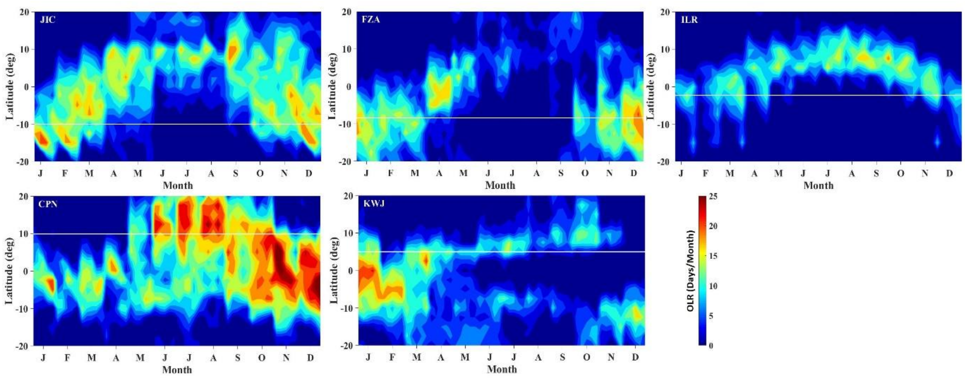

Figure 8: Monthly distribution of the OLR occurrence frequency plotted as a function of the geographic latitude (dip equator indicated by a white line) for each of the stations.

There has been an extensive discussion on the geometry and coupling of the upward propagating GW considered most suitable for the ESF initiation (Krall et al., 2013a; Tsunoda, 2010b, 2010c). The seeding of plasma irregularity is expected to occur when the phase front of the GW becomes aligned with the magnetic field line ($\vec{B}$). This alignment condition is considered possible, only if the convective active regions are located close to the magnetic dip equator (Tsunoda, 2010a). Figure 8. shows the variation of the monthly averaged OLR distribution across the five stations. With the measurement taken over 10 degrees longitudinal range which brackets the location of the ionosonde station and ± 20 degrees at both sides of the dip equator (white line). The defined threshold OLR strength used to distinguish regions of convective and non-convective activity was 200 W/m^2 in each bin per day (Gu and Zhang, 2002). The frequency of the OLR occurrences represents the frequency of the GW occurrences in each month. In the regions where the dip equator is located at the southern hemisphere, we noticed that the GW occurrence peak during the J-solstice is located farther from the dip equator compared to the D-solstice. The observed pattern of the monthly GW distribution displayed a tendency to produce a solstitial asymmetry in the expected seeding effect on the ESF occurrence. On the other hand, a large OLR occurrence frequency was observed close to the dip equator from January to November at the KWJ longitude. While throughout the year, a varying degree of large OLR occurrence was observed around the dip equator at the CPN longitude. A comparison between the OLR occurrence frequency and the RSF occurrence percentage (Figure 4) shows a strong agreement at all the longitudes except the CPN station. Where the observed low RSF occurrence percentage contradicts the large OLR frequency around the dip equator in the region.

Apart from the requisite GW and $\vec{B}$ alignment, a large local electron density was also described as an important prerequisite for the large ESF growth (Krall et al., 2013b). The large electron density is considered necessary to support the GW induced electric field and the plasma instability growth. The relationship between the perturbation wind and the induced electric field is expressed as (Abdu et al., 2009; Tsunoda, 2010b);

$$\delta \boldsymbol{J} = \sigma_P(\delta \boldsymbol{E} + \delta \boldsymbol{U} \times \boldsymbol{B}) = 0 \quad (3)$$

$$\delta \boldsymbol{E} = -(\delta \boldsymbol{U} \times \boldsymbol{B}) \quad (4)$$

Where σ_P is the Pedersen conductivity, $\delta \boldsymbol{U}$ is the perturbation wind velocity due to gravity wave, $\delta \boldsymbol{E}$ is the perturbation electric field and $\boldsymbol{B}$ is the magnetic field. The total electric field is assumed to be a sum of the ambient and perturbation electric field. In the absence of the ambient electric field, the vertical velocity drift induced by the perturbation $\boldsymbol{E}$ field can be expressed as $V = {}^{v_{in}}/_{\Omega}\left({}^{\delta \boldsymbol{E}}/_{\boldsymbol{B}}\right)$.

Ann. Geophys. Discuss., https://doi.org/10.5194/angeo-2019-24
Manuscript under review for journal Ann. Geophys.
Discussion started: 27 February 2019

In the case of the West African sector, past studies (Okoh et al., 2017; Yizengaw et al., 2013) have presented a similar discussion about the role of GW in the observed large RSF occurrence during a solstice month. Yizengaw et al., (2013) attributed the post-midnight enhancement of the eastward polarization electric field in the West African region to the presence of the localized charged particle. These dust particles are generated by the strong gusty wind that characterizes the harmattan season in the region. The particles are dispersed into higher altitude, where the associated friction becomes the source of the polarized electric charges and subsequently enhances zonal E field. Thus, the perturbation electric field further increases the vertical plasma vortex flow in the evening ionosphere and the subsequent initiation of the R-T instability process. The presence of a more frequently active ITCZ is expected to enhance the plasma irregularity seeding in a region (Li et al., 2016). This complementary role of the GW induced zonal E field and the observed monthly distribution pattern of the convective region is found to be consistent with the solstice asymmetry in the ESF occurrence. Such a similar mechanism is expected to be applicable to the other four longitudinal sectors during seasons where intense convective activity is observed near the magnetic dip equator. However, considering the negative correlation between the OLR frequency and RSF occurrence at the CPN station, we highlight the F region electrodynamics in the Asian sector. Figure 4 of Vichare and Richmond, (2005) presented a zonal variation of PRE in comparison with the magnetic field strength, field line integrated Pedersen conductivity and zonal E field. The weakest PRE were recorded in the longitudinal range 90^{o}E – 120^{o}E and 160^{o}E – 240^{o}E, which encloses the CPN and KWJ stations respectively. The recorded weak PRE in the former longitude sector could be attributed to the combined effect of large magnetic field strength and a small field line integrated conductivities. While the later longitude range was shown to have the minimum zonal E field, which correlates with the generally weak PSSR observed in these regions during the LSA (Figure 7b.). Hence, the negative or weak correlation observed in both sectors is associated with the unfavourable background ionospheric condition for the plasma irregularity growth. It is important to note that the observed solstitial asymmetry in ESF occurrence becomes more

Ann. Geophys. Discuss., https://doi.org/10.5194/angeo-2019-24
Manuscript under review for journal Ann. Geophys.
Discussion started: 27 February 2019

Annales Geophysicae Discussions
Open Access
EGU

prominent at the CPN station during the MSA, which correlates with a significant increase in the local electron density. Likewise, the ESF occurrence percentage increases significant at the KWJ during the J-solstice, which is uncorrelated with the percentage increase of the PSSR in relation to the solar flux dependence. These are considered as an evidence of improved seeding of the plasma instability growth triggered by a substantial increase in the local electron density.

5. Conclusion

The statistical result of the hourly variation of the RSF occurrence percentage across different longitude sectors was investigated during the MSA and LSA period for stations close to the magnetic equator. The manual observation of the seasonal variation of the RSF occurrence pattern using the ionogram data revealed the distinct RSF occurrence features at each of the regions. This highlighted the complex morphology of the ESF events and the diverse role of the different factors contributing to plasma irregularity initiation across the different longitudes during the MSA and LSA. The West African region (ILR) has the highest average ESF occurrence percentage across the four seasons during the LSA period, even when the ambient ionospheric condition is less conducive for the R-T instability growth. Other important observations included the varying longitudinal pattern of the equinox asymmetry during the LSA and MSA. The observed inconsistency in the asymmetry pattern requires further investigation to understand the factors responsible for the changes in the equinoctial season maximum during the different solar epochs. Likewise, an anti-solar activity variation of the ESF occurrence percentage was also observed at the JIC and FZA stations during the S-equinox. This was attributed to the possible role of an expected increase in the bottom-side density scale length with the solar flux index. Finally, the observed solstice asymmetry in the low declination angle region and the PRE peak deviation from the expected STBA ratio were associated with the presence of a strong convective activity around the dip equator. The described GWBA theory proved to be a sufficient explanation for the observed discrepancy in the seasonal variation of ESF occurrence in relation with the STBA theory. Hence, the seed perturbation effect was considered as an important factor enhancing the plasma irregularity growth during unfavourable ambient ionospheric condition.

Acknowledgement

References

Abdu, M. A.: Outstanding problems in the equatorial ionosphere-thermosphere electrodynamics relevant to spread F, J. Atmos. Solar-Terrestrial Phys., 63(9), 869–884, doi:10.1016/S1364-6826(00)00201-7, 2001.

Abdu, M. A., Bittencourt, J. A. and Batista, I. S.: Magnetic declination control of the equatorial F region dybamo electric field development and spread F, Jgr, 86(A13), 143–1446, doi:10.1029/JA086iA13p11443, 1981.

Abdu, M. A., Batista, I. S. and Sobral, J. H. A.: A New Aspect of Magnetic Declination Control of Equatorial Spread F and F Region Dynamo, J. Geophys. Res. Sp. Phys., 97(A10), 14,897-14,904, doi:10.1029/92JA00826, 1992.

Abdu, M. A., Alam Kherani, E., Batista, I. S., De Paula, E. R., Fritts, D. C. and Sobral, J. H. A.: Gravity wave initiation of equatorial spread F/plasma bubble irregularities based on observational data from the SpreadFEx campaign, Ann. Geophys., 27(7), 2607–2622, doi:10.5194/angeo-27-2607-2009, 2009.

Basu, S., Basu, S., Aarons, J., McClure, J. P. and Cousins, M. D.: ON THE COEXISTENCE OF KILOMETER- AND METER-SCALE IRREGULARITIES IN THE NIGHTTIME EQUATORIAL F REGION., J Geophys Res, 83(A9), 4219–4226, doi:10.1029/JA083iA09p04219, 1978.

Batista, I. S., Abdu, M. A. and Bittencourt, J. A.: Equatorial F region vertical plasma drifts: Seasonal and longitudinal asymmetries in the American sector, J. Geophys. Res. Sp. Phys., 91(A11), 12055–12064, doi:10.1029/JA091iA11p12055, 1986.

Booker, H. G. and Wells, H. W.: Scattering of radio waves by the F -region of the ionosphere, J. Geophys. Res., 43(3), 249, doi:10.1029/TE043i003p00249, 1938.

Bowman, G. G.: A review of some recent work on mid-latitude spread-F occurence as detected by ionosondes, J. Geomag. Geoelectr., 42, 109–138, 1990.

Dabas, R. S., Singh, L., Lakshmi, D. R., Subramanyam, P., Chopra, P. and Garg, S. C.: Evolution and dynamics of equatorial plasma bubbles: Relationships to ExB drift, postsunset total electron content enhancements, and equatorial electrojet strength, Radio Sci., 38(4), n/a-n/a, doi:10.1029/2001RS002586, 2003.

Eccles, J. V., St. Maurice, J. P. and Schunk, R. W.: Mechanisms underlying the prereversal enhancement of the vertical plasma drift in the low-latitude ionosphere, J. Geophys. Res. Sp. Phys., 120(6), 4950–4970, doi:10.1002/2014JA020664, 2015.

Fejer, B. G., Scherliess, L. and de Paula, E. R.: Effects of the vertical plasma drift velocity on the generation and evolution of equatorial spread F, J. Geophys. Res. Sp. Phys., 104(A9), 19859–19869, doi:10.1029/1999JA900271, 1999.

Gentile, L. C., Burke, W. J. and Rich, F. J.: A global climatology for equatorial plasma bubbles in the topside ionosphere, Ann. Geophys., 24(1), 163–172, doi:10.5194/angeo-24-163-2006, 2006.

Gu, G. and Zhang, C.: Cloud components of the Intertropical Convergence Zone, J. Geophys. Res. Atmos., doi:10.1029/2002JD002089, 2002.

Heelis, R. A.: Electrodynamics in the low and middle latitude ionosphere: A tutorial, J. Atmos. Solar-Terrestrial Phys., 66(10), 825–838, doi:10.1016/j.jastp.2004.01.034, 2004.

Hoang, T. L., Abdu, M. A., MacDougall, J. and Batista, I. S.: Longitudinal differences in the equatorial spread F characteristics between Vietnam and Brazil, Adv. Sp. Res., 45(3), 351–360, doi:10.1016/j.asr.2009.08.019, 2010.

Huang, C. and Kelley, M. C.: Nonlinear evolution of equatorial spread F : 4. Gravity waves, velocity shear, and day-to-day variability, J. Geophys. Res., 101(A11), 24521, doi:10.1029/96JA02332, 1996.

Huang, C. S.: The characteristics and generation mechanism of small-amplitude and large-amplitude ESF irregularities observed by the C/NOFS satellite, J. Geophys. Res. Sp. Phys., 122(8), 8959–8973, doi:10.1002/2017JA024041, 2017.

Huang, C. S.: Effects of the postsunset vertical plasma drift on the generation of equatorial spread F, Prog. Earth Planet. Sci., 5(1), doi:10.1186/s40645-017-0155-4, 2018.

Klinngam, S., Supnithi, P., Rungraengwajiake, S., Tsugawa, T., Ishii, M. and Maruyama, T.: The occurrence of equatorial spread-F at conjugate stations in Southeast Asia, Adv. Sp. Res., 55(8), 2139–2147, doi:10.1016/j.asr.2014.10.003, 2015.

Krall, J., Huba, J. D. and Fritts, D. C.: On the seeding of equatorial spread F by gravity waves, Geophys. Res. Lett., 40(4), 661–664, doi:10.1002/grl.50144, 2013a.

Krall, J., Huba, J. D., Joyce, G. and Hei, M.: Simulation of the seeding of equatorial spread F by circular gravity waves, Geophys. Res. Lett., 40, 1–5, doi:10.1029/ 2012GL054022, 2013b.

Lee, C. C.: Occurrence and onset conditions of postsunset equatorial spread F at Jicamarca during solar minimum and maximum, J. Geophys. Res. Sp. Phys., 115(10), 1–7, doi:10.1029/2010JA015650, 2010.

Li, G., Ning, B., Liu, L., Ren, Z., Lei, J. and Su, S.-Y.: The correlation of longitudinal/seasonal variations of evening equatorial pre-reversal drift and of plasma bubbles, in Annales Geophysicae, vol. 25, pp. 2571–2578., 2008.

Li, G., Ning, B., Abdu, M. A., Yue, X., Liu, L., Wan, W. and Hu, L.: On the occurrence of postmidnight equatorial F region irregularities during the June solstice, J. Geophys. Res. Sp. Phys., 116(4), 1–19, doi:10.1029/2010JA016056, 2011.

Li, G., Otsuka, Y., Ning, B., Abdu, M. A., Yamamoto, M., Wan, W., Liu, L. and Abadi, P.: Enhanced ionospheric plasma bubble generation in more active ITCZ, Geophys. Res. Lett., doi:10.1002/2016GL068145, 2016.

Manju, G. and Madhav Haridas, M. K.: On the equinoctial asymmetry in the threshold height

Ann. Geophys. Discuss., https://doi.org/10.5194/angeo-2019-24
Manuscript under review for journal Ann. Geophys.
Discussion started: 27 February 2019

Annales Geophysicae Discussions Open Access EGU

for the occurrence of equatorial spread F, J. Atmos. Solar-Terrestrial Phys., 124, 59–62, doi:10.1016/j.jastp.2015.01.008, 2015.

Maruyama, T., Saito, S., Kawamura, M. and Nozaki, K.: Thermospheric meridional winds as deduced from ionosonde chain at low and equatorial latitudes and their connection with midnight temperature maximum, J. Geophys. Res. Sp. Phys., 113(9), 1–9, doi:10.1029/2008JA013031, 2008.

Ogawa, T., Otsuka, Y., Shiokawa, K., Saito, A. and Nishioka, M.: Ionospheric disturbances over Indonesia and their possible association with atmospheric gravity waves from the troposphere, J. Meteorol. Soc. JAPAN, doi:10.2151/jmsj.84A.327, 2006.

Okoh, D., Rabiu, B., Shiokawa, K., Otsuka, Y., Segun, B., Falayi, E., Onwuneme, S. and Kaka, R.: First Study on the Occurrence Frequency of Equatorial Plasma Bubbles over West Africa Using an All-Sky Airglow Imager and GNSS Receivers, J. Geophys. Res. Sp. Phys., 122(12), 12430–12444, doi:10.1002/2017JA024602, 2017.

Ossakow, S. L.: Spread-F theories-a review, J. Atmos. Terr. Phys., 43(5–6), 437–452, doi:10.1016/0021-9169(81)90107-0, 1981.

De Paula, E. R., Muella, M. T. A. H., Sobral, J. H. A., Abdu, M. A., Batista, I. S., Beach, T. L. and Groves, K. M.: Magnetic conjugate point observations of kilometer and hundred-meter scale irregularities and zonal drifts, J. Geophys. Res. Sp. Phys., 115(8), doi:10.1029/2010JA015383, 2010.

Pezzopane, M., Zuccheretti, E., Abadi, P., De Abreu, A. J., De Jesus, R., Fagundes, P. R., Supnithi, P., Rungraengwajiake, S., Nagatsuma, T., Tsugawa, T., Cabrera, M. A. and Ezquer, R. G.: Low-latitude equinoctial spread-F occurrence at different longitude sectors under low solar activity, Ann. Geophys., 31(2), 153–162, doi:10.5194/angeo-31-153-2013, 2013.

Pietrella, M., Pezzopane, M., Fagundes, P. R., Jesus, R. De, Supnithi, P., Klinngam, S., Ezquer, R. G. and Cabrera, M. A.: Journal of Atmospheric and Solar-Terrestrial Physics Equinoctial spread-F occurrence at low latitudes in different longitude sectors under moderate and high solar activity, J. Atmos. Solar-Terrestrial Phys., 164(July), e815–e818, doi:10.1016/j.jastp.2017.07.007, 2017.

Qian, L., Solomon, S. C. and Kane, T. J.: Seasonal variation of thermospheric density and composition, J. Geophys. Res. Sp. Phys., 114(1), doi:10.1029/2008JA013643, 2009.

Reinisch, B. W. and I. A. Galkin: Global ionospheric radio observatory (GIRO), Earth, Planets Sp., 63, 377–381, doi:10.5047/eps2011.03.001.2011, 2011.

Shi, J. K., Wang, G. J., Reinisch, B. W., Shang, S. P., Wang, X., Zherebotsov, G. and Potekhin, A.: Relationship between strong range spread F and ionospheric scintillations observed in Hainan from 2003 to 2007, J. Geophys. Res. Sp. Phys., 116(8), 1–5, doi:10.1029/2011JA016806, 2011.

Smith, J. M., Rodrigues, F. S., Fejer, B. G. and Milla, M. A.: Coherent and incoherent scatter radar study of the climatology and day-to-day variability of mean F region vertical drifts and equatorial spread F, J. Geophys. Res. A Sp. Phys., 121(2), 1466–1482, doi:10.1002/2015JA021934, 2016.

Stolle, C., Lür, H. and Fejer, B. G.: Relation between the occurrence rate of ESF and the

Ann. Geophys. Discuss., https://doi.org/10.5194/angeo-2019-24
Manuscript under review for journal Ann. Geophys.
Discussion started: 27 February 2019

Annales Geophysicae Discussions Open Access EGU

equatorial vertical plasma drift velocity at sunset derived from global observations, Ann. Geophys., 26(12), 3979–3988, doi:10.5194/angeo-26-3979-2008, 2008.

Su, S.-Y., Chao, C. K. and Liu, C. H.: On monthly/seasonal/longitudinal variations of equatorial irregularity occurrences and their relationship with the postsunset vertical drift velocities, J. Geophys. Res. Sp. Phys., 113(A5), 2008.

Su, S. Y., Chao, C. K., Liu, C. H. and Ho, H. H.: Meridional wind effect on anti-solar activity correlation of equatorial density irregularity distribution, J. Geophys. Res. Sp. Phys., 112(10), 1–11, doi:10.1029/2007JA012261, 2007.

Su, S. Y., Chao, C. K. and Liu, C. H.: Cause of different local time distribution in the postsunset equatorial ionospheric irregularity occurrences between June and December solstices, J. Geophys. Res. Sp. Phys., 114(4), doi:10.1029/2008JA013858, 2009.

Sultan, P. J.: Linear theory and modeling of the Rayleigh-Taylor instability leading to the occurrence of equatorial spread F, J. Geophys. Res., 101(A12), 26875, doi:10.1029/96JA00682, 1996.

Tsunoda, R. T.: On equatorial spread F: Establishing a seeding hypothesis, J. Geophys. Res. Sp. Phys., 115(12), doi:10.1029/2010JA015564, 2010a.

Tsunoda, R. T.: On seeding equatorial spread F: Circular gravity waves, Geophys. Res. Lett., 37(10), doi:10.1029/2010GL043422, 2010b.

Tsunoda, R. T.: On seeding equatorial spread F during solstices, Geophys. Res. Lett., doi:10.1029/2010GL042576, 2010c.

Tsunoda, R. T., Nguyen, T. T. and Le, M. H.: Effects of tidal forcing, conductivity gradient, and active seeding on the climatology of equatorial spread F over Kwajalein, J. Geophys. Res. Sp. Phys., 120(1), 632–653, doi:10.1002/2014JA020762, 2015.

Vichare, G. and Richmond, A. D.: Simulation study of the longitudinal variation of evening vertical ionospheric drifts at the magnetic equator during equinox, J. Geophys. Res. Sp. Phys., 110(A5), 1–8, doi:10.1029/2004JA010720, 2005.

Waliser, D. E. and Gautier, C.: A satellite-derived climatology of the ITCZ, J. Clim., doi:10.1175/1520-0442(1993)006<2162:ASDCOT>2.0.CO;2, 1993.

Wang, G. J., Shi, J. K., Wang, Z., Wang, X., Romanova, E., Ratovsky, K. and Polekh, N. M.: Solar cycle variation of ionospheric parameters over the low latitude station Hainan, China, during 2002–2012 and its comparison with IRI-2012 model, Adv. Sp. Res., 60(2), 381–395, doi:10.1016/j.asr.2016.12.013, 2017.

Whalen, J. A.: Dependence of equatorial bubbles and bottomside spread F on season, magnetic activity, and e ?? B drift velocity during solar maximum, J. Geophys. Res. Sp. Phys., 107(A2), doi:10.1029/2001JA000039, 2002.

Woodman, R. F. and La Hoz, C.: RADAR OBSERVATIONS OF F REGION EQUATORIAL IRREGULARITIES., J Geophys Res, 81(31), 5447–5466, doi:10.1029/JA081i031p05447, 1976.

Yizengaw, E., Retterer, J., Pacheco, E. E., Roddy, P., Groves, K., Caton, R. and Baki, P.: Postmidnight bubbles and scintillations in the quiet-time June solstice, Geophys. Res. Lett., 40(21), 5592–5597, doi:10.1002/2013GL058307, 2013.